Chiang Mai J. Sci. 2023; 50(2): 1-17
https://doi.org/10.12982/CMJS.2023.015
Journal homepage : http://epg.science.cmu.ac.th/ejournal/

Research Article

Experimental and Semi-Phenomenological Investigation on Sound Absorption Performance of Natural Granular Sound Absorber: A Case Study on Rice Bran Composites

Purintorn Chanlert*[a], Wiparat Manoma [a], Aneeta Jintara [a], Thanate Kerdkaew [b], and Thana Sutthibutpong [c]

[a] Faculty of Science and Technology, Songkhla Rajabhat University, Songkhla 90000 Thailand

[b] Chemistry and Biology Unit, Institute for the Promotion of Teaching Science and Technology, Bangkok 10110, Thailand

[c] Theoretical and Computational Physics Group, Department of Physics, Faculty of Science, King Mongkut's University of Technology Thonburi, Bangkok 10140, Thailand

*Author for correspondence; e-mail: purintorn.ch@skru.ac.th

Received: 26 November 2022
Revised: 7 February 2023
Accepted: 9 February 2023

Abstract

The sound absorption performance of rice bran composites was quantitatively investigated through an improved semi-phenomenological approach. Rice bran (RB) was employed as the primary and structural component in the creation of granular-type sound absorbers with urea-formaldehyde (UF) adhesive. The sound absorption coefficient (SAC) was measured by the two-microphone impedance tube method. Samples with a rice bran per volume ratio lower than 253 kg/m^3 show peak-valley characteristics in the saturation region of their SAC spectrum. Five non-acoustic parameters for each sample were obtained by direct measurement and fitting the experimental SACs to the semi-phenomenological Johnson-Champoux-Allard (JCA) equivalent fluid model using the least-squares fitting method. Samples with higher proportions of RB demonstrate lower porosity (ϕ), viscous characteristic length (Λ), and thermal characteristic length (Λ'). Flow resistivity (σ) was the only parameter that noticeably increases when RB increased while tortuosity (α_∞) did not show a strong correlation. For the uncertainty analysis of the experimental SAC, multivariate method was used in this study. A new model (NM) was predicated on the power-law relation introduced by Delany and Bazley, in which the SAC was a function of flow resistivity alone. The new model predicted the SAC of RB composites more precisely than the standard Delany-Bazley model ($\overline{\Delta}_{\text{abs(DBM)}} \approx 4.0\overline{\Delta}_{\text{abs(NM)}}$). The proposed model had the potential to be extended into a more unified empirical model of SAC for granular-typed sound absorbers in future investigations with a broader spectrum of granular materials.

Keywords: rice bran composites, granular sound absorber, sound absorption coefficient, Johnson-Champoux-Allard model, transfer matrix method, multivariate method, flow resistivity, empirical model

1. Introduction

Rock wool and glass wool are synthetic fibers that have been utilized for decades in the sector of sound absorption [1] since they are typically utilized in buildings to minimize sound echo and reverberation. Nevertheless, the production and use of these substances have detrimental effects on the health of individuals who are frequently exposed to them [2]. These compounds have substantial environmental effects because they are difficult to eliminate [3]. Researchers are interested in natural materials that can serve as alternatives to synthetic ones. According to the study by Koizumi et al. [4], the apparent density, thickness, and fiber diameter were utilized as variables to investigate the sound-absorbing characteristics of bamboo fiber. The finding indicates that bamboo fiber can be employed as a sound absorber because its sound absorption coefficient (SAC) is comparable to that of synthetic materials like glass wool. This finding inspired researchers to investigate the potential of natural acoustic materials. Sound absorption properties of single-component natural absorbers such as coconut coir [5], and palmyra palm fruit fibers [6] are shown to have acceptable sound absorption abilities. Additionally, there are multicomponent natural sound absorbers with respectable sound absorption capabilities including the composites of rice straw-wood [7], rice hull-sawdust [8], and coconut coir-rice husk [9].

Rice (*Oryza sativa* L.) is cultivated worldwide under a range of agronomic conditions, most notably in Asia. Furthermore, rice grains are a well-known food source, with more than half of the world's population consuming them daily [10]. The endosperm of a rice grain is surrounded by a thin layer of rice bran (RB), which is then covered by a solid husk. Rice retains rice bran after the husk has been removed, which imparts the grain's brown color due to direct air contact with rice bran. Rice bran is estimated to account approximately for 12% of the total weight of rice after milling procedures [11], and it is commonly categorized as agricultural waste. Rice bran is typically transformed or added as a component to numerous products, such as animal feed, cooking oil, or organic fertilizer [12], with a potential application in supplemental diet and cosmetic manufacturing. However, the application of rice bran in other sectors is largely unknown. Unlike other rice by-products such as straw and husk, rice bran has received less attention in terms of its possible utility in the production of sound-absorbing materials [13]. Because of its granular characteristics, rice bran might be a good candidate element for manufacturing good natural porous-type sound absorbers.

To optimize the acoustic properties of porous materials, it is necessary to explore the relationship between structural factors and acoustic behavior. In general, porous media assuming simple internal structure, such as straight cylindrical pores, necessitates a simpler model than one with non-uniform cross-sections. The semi-phenomenological models, such as the Johnson-Champoux-Allard (JCA) model [14,15], require five non-acoustic parameters including flow resistivity (σ), porosity (ϕ), tortuosity (α_∞), viscous characteristic lengths (Λ), and thermal characteristic length (Λ'). However, some researchers including Delany-Bazley [16], and Garai-Pompoli [17] established an empirical model for predicting the SAC spectrum that requires just one parameter, the airflow resistivity (σ). It was recognized that these empirical models were derived from the SAC spectra of several fibrous-type absorbers, such as glass wool [16] or polyester fiber [17]. Few empirical models of granular-type sound absorbers have been investigated before this study [18].

The materials studied in this research, rice bran composites, represent a unique and original contribution to the field of natural sound absorber. It represents a significant advancement in academic research as it shows the investigation on the sound absorption capabilities and mathematical expressions of granular rice bran composites. Section 2 addresses material preparation and measurements of flow resistivity, porosity, and sound absorption coefficient. Section 3 contains the results and discussion. Section 3.1 provides an overview of the rice bran composites. Subsection 3.2 describes the explanation of the sound absorption capacity of rice bran composites. The investigation of non-acoustic parameters derived from the least-squares fitting of the JCA equivalent fluid model is presented in Section 3.3 [14,15]. The uncertainty analysis of the SAC is presented in Section 3.4, utilizing the multivariate method. Section 3.5 presents a new empirical model that predicts the sound absorption properties of granular rice bran composites and compares it to the Delany-Bazley model, which is one of the most well-known empirical models associated with the sound absorption of porous materials. Finally, the conclusion of this study is provided in section 4.

2. MATERIALS AND METHOD

2.1 Sample Preparation

Rice bran (RB) was collected from local rice millers in Songkhla province, Thailand. Before the sample-making process, rice bran was dried inside a convection oven at 100 °C for 120 minutes. Urea-formaldehyde (UF) is a thermosetting polymer extensively used in various wood industries. In this study, commercial UF adhesive powder (Bosny Co., UK) was used. The ratio of UF powder adhesive to water was fixed at 2:1, correspondingly. Warning: Urea-formaldehyde (UF) adhesive is a volatile compound. It has been linked to an increased risk of rhynopharyngeal cancer [19] and should be handled with caution. It is important to follow proper safety precautions when working with UF adhesive, including wearing protective gear and ensuring proper ventilation.

The samples were prepared by combining the rice bran and UF adhesive. The diameter of the cylindrical sample was fixed at 28.6 mm to make it suitable for measuring sound absorption. The thickness of all samples was controlled to a uniform 40 mm for consistency. Rice bran contents were varied from 4.5, 5.5, 6.5, 7.5, and 8.5 g per unit volume representing rice bran mass per volume ratios ($D_{\mathrm{RB}} = m_{\mathrm{RB}}/V$) of 175, 214, 253, 292, and 331 kg/m^3, respectively. In the same manner, two sets from different adhesive contents were made using 6 g and 8 g of UF adhesive powder per unit volume representing adhesive mass per volume ratios ($D_{\mathrm{UF}} = m_{\mathrm{UF}}/V$) of 233 and 311 kg/m^3, respectively. Rice bran, UF adhesive powder, and water were adequately mixed inside a bowl before putting it into a cylindrical metal mold. Since the rice bran composites usually overflowed from the mold edge, a sufficient load was placed above the mold to keep the mixture volumetric controlled. Then, the wet samples were put inside the convection oven set to 100 °C for 90 minutes. The bulk density and other physical parameters of ten distinctive formulae (RB-1a ~ RB-5b) were measured and investigated after the sample's mass becomes constant.

2.2 Flow Resistivity and Porosity Measurement

Flow resistivity (σ) is the property that determines how air flows through porous media. Flow resistivity is one of the primary elements that influence the sound absorption of materials. According to ISO9053-1 [20], static flow resistivity of the air can be determined from the slope of the relationship between the varying volumetric flow rate (Q) of the air passing through the porous sample and the pressure difference (ΔP) between two sides of the specimen according to the linear equation:

$$Q = \left(\frac{A}{\sigma L}\right)\Delta P \tag{1}$$

where A and L represent the cross-sectional area and thickness of the sample, respectively. Figure 1 depicts the schematic diagram of the flow resistivity measurement system. The measured flow resistivity values are shown in Table 2.

Porosity (ϕ) is one of the primary factors influencing the sound absorption capacity of the material. Porosity was estimated in this study using sample bulk density (ρ_{bulk}) and absolute density of the solid phase (ρ_{abs}) as follows:

$$\phi = 1 - \frac{\rho_{\mathrm{bulk}}}{\rho_{\mathrm{abs}}} \tag{2}$$

In this study, the solid phase of the porous materials is composed of two components: rice

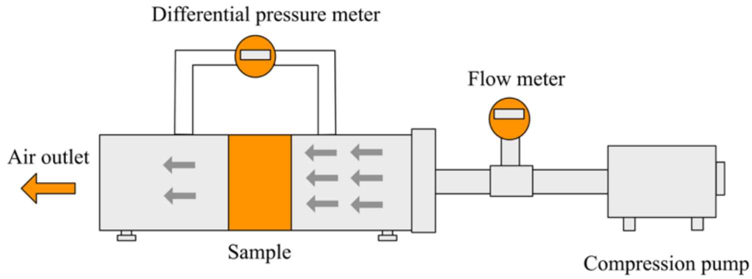

Figure 1. Schematic diagram of flow resistivity measurement system.

bran and UF adhesive. Using a water pycnometer, the absolute density of rice bran was determined [21]. Before measuring, rice bran was ground into the finest powder possible. To successfully eliminate air bubbles from rice bran, a pycnometer flask containing rice bran powder and water was placed in an ultrasonic bath at 60 °C for 60 minutes. Finally, the measured absolute density of the rice bran (ρ_{RB}) was estimated to be 2,518 kg/m^3. Utilizing the same technique, the absolute density of cured UF adhesive (ρ_{UF}) was measured to be 1,282 kg/m^3. Lastly, the absolute density of the solid phase can be determined by:

$$\rho_{\mathrm{abs}} = \frac{\rho_{\mathrm{RB}} D_{\mathrm{RB}} + \rho_{\mathrm{UF}} D_{\mathrm{UF}}}{D_{\mathrm{RB}} D_{\mathrm{UF}}} \tag{3}$$

where D_{RB} and D_{UF} represent the mass per unit volume of the rice bran and UF adhesive, respectively, as displayed in Table 1. The porosity obtained from Eq. 2 were listed in Table 2.

2.3 Sound Absorption Coefficient Measurement

A two-microphone cylindrical impedance tube built specifically based on ASTM E1050-98 [22] and ISO 10534-2 [23] standards was used to evaluate the normal-incident sound absorption coefficient (SAC) spectra of the materials. Based on Koruk's study [24], a single-size impedance tube can be utilized in the measurement of the SAC spectrum of low and high frequencies at the acceptable precision of the well-established double-size impedance tubes. In this study, the cylindrical-shaped impedance tube has a 28.6 mm internal diameter [25], and the tube's body was made of stainless steel to protect the inside from external background noise. Two 1/4-inch laboratory-graded measurement microphones (GRAS 40PP; GRAS Sound & Vibration, Denmark) were placed and sealed, with the microphone tips positioned against the tube wall as illustrated in Figure 2.

A full-range speaker was put at the tube's end as a sound source to create noise at a wide-frequency range within the impedance tube. With a tube length of 1000 mm, the sound is expected to become plane waves while approaching the sample's surface. The cylinder-shaped sample was firmly put into the sample holder at the tube's other end. In the sample holder, a hard backing plate was placed behind the sample. A data acquisition device (NI-9230; National Instruments, TX, USA) was used to capture the signals from both measurement microphones as displayed in Figure 3.

The transfer function (H_{12}) between signals obtained from two microphones was then examined using the data acquisition module explicitly made for Python. The following equation describes the calculation of SAC (α) from the transfer function of two microphone signals:

$$R = \frac{H_{12} - e^{-ik_0 s}}{e^{ik_0 s} - H_{12}} e^{2ik_0(s+l)} \tag{4}$$

$$\mathrm{SAC} = 1 - |R|^2 \tag{5}$$

Table 1. Sample information.

Sample	D_{RB} (kg/m^3)	D_{UF} (kg/m^3)	ρ_{bulk} (kg/m^3)	NRC
RB-a1	175	233	378	0.57
RB-a2	214	233	416	0.57
RB-a3	253	233	459	0.47
RB-a4	292	233	486	0.38
RB-a5	331	233	522	0.32
RB-b1	175	311	459	0.53
RB-b2	214	311	502	0.53
RB-b3	253	311	545	0.52
RB-b4	292	311	580	0.34
RB-b5	331	311	615	0.30

Table 2. Non-acoustic parameters obtained from the least-square fitting of the JCA model and transfer matrix method.

Sample	σ^* (Pa·s·m^{-2})	ϕ^{**}	α_∞	Λ (μm)	Λ' (μm)	f_c (kHz)	$\delta_c/2$ (μm)
RB-a1	12210	0.792	1.030	31.3	517.2	1.16	31.3
RB-a2	33282	0.778	1.000	18.8	447.0	3.19	18.8
RB-a3	96364	0.761	1.000	14.0	547.0	9.03	11.9
RB-a4	168171	0.753	1.000	4.0	30.5	15.59	8.5
RB-a5	283867	0.740	1.000	3.0	26.8	25.86	6.6
RB-b1	6985	0.734	1.170	32.6	1102.6	0.54	45.8
RB-b2	22908	0.719	1.000	14.6	880.1	2.03	23.6
RB-b3	59360	0.703	1.000	13.0	333.6	5.14	14.8
RB-b4	178758	0.692	1.000	3.9	31.7	15.23	8.6
RB-b5	328733	0.680	1.000	3.6	29.9	27.52	6.4

* σ were obtained from the measurement according to ISO9053-1 [20].
** ϕ was estimated from Eq. 2 referring to [6].

where R is a complex sound reflection coefficient, i is the imaginary number $\sqrt{-1}$, k_0 is the wavenumber of the sound wave, l is the distance between the nearest microphone (Mic 2) and the sample surface (75.03 ± 0.06 mm), s is the distance between two microphones (30.07 ± 0.12 mm). The SAC measurement was performed under the ambient temperature of 27.0 ± 1.8 °C. In this study, SAC was calculated based on the average transfer function of three samples (N = 3), each having the same formula of Rice Bran (RB) and adhesive. SAC spectra were obtained using the measurement with air gaps of 0 mm, 20 mm, and 40 mm since these air gaps can reduce the

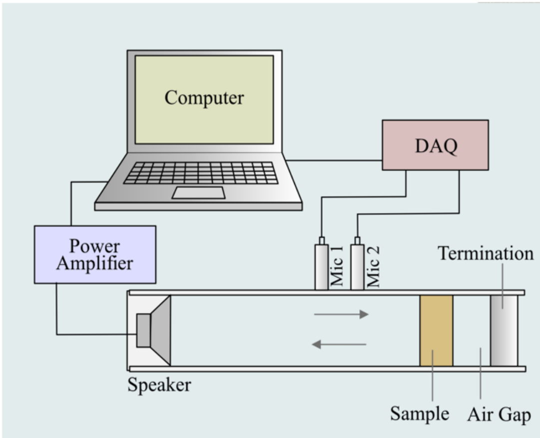

Figure 2. Schematic diagram of two-microphone impedance tube.

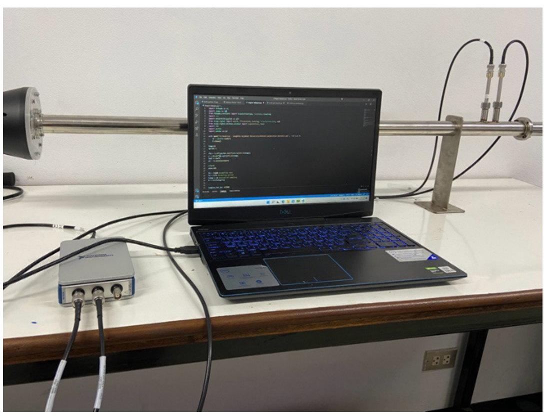

Figure 3. Impedance tube setting.

uncertainty of the least-squares fitting of the Johnson-Champoux-Allard (JCA) equivalent fluid model to experimental SAC spectra. The determination of non-acoustic parameters and the new empirical model for SAC are described in the following section.

3. Results and Discussion

3.1 Sample Characteristics

The microstructure of rice bran composites was thoroughly studied in sample RB-a1 using a Scanning Electron Microscope (SEM), as shown in Figure 4. The images showed that the rice bran granules varied in size but were almost spherical and angular in shape. rice bran composes of the aleurone layer, tegmen, and pericarp [11]. These structures are made up of a variety of organic compounds, the majority of which are carbohydrates [11] such as cellulose and hemicellulose [26]. Numerous pores surrounded by cell walls are detected in rice bran fractures, according to SEM pictures. As a result, the porous nature of rice bran can be advantageous in the production of sound absorption materials.

Table 1 lists sample information, including the sample name, rice bran (D_{RB}) and UF adhesive (D_{UF}) mass per unit volume, and sample bulk density (ρ_{bulk}) of ten distinctive samples. According to Table 1, the sample bulk density is directly proportional to rice bran and adhesive contents. RB-b5, having the highest rice bran and

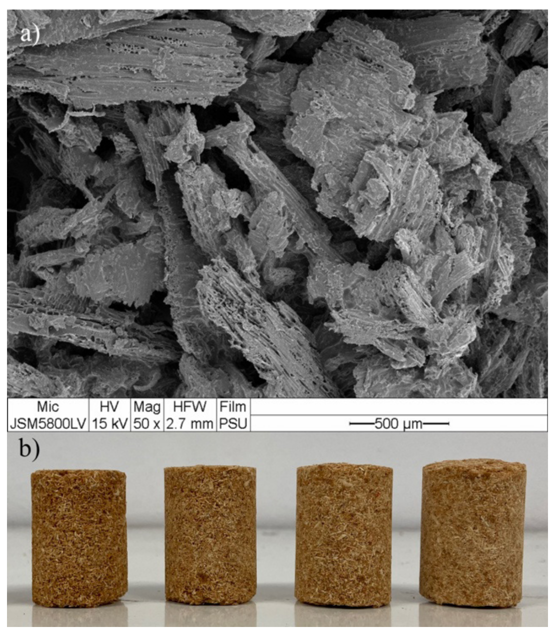

Figure 4. Scanning electron microscope (SEM) image showing the surface morphology of rice bran composites (RB-a1) a). Photo image of rice bran samples prepared for impedance tube testing b).

adhesive content, demonstrates the highest bulk density (615 kg/m^3). In contrast, because RB-a1 has the least amount of rice bran and adhesive, it has the lowest bulk density (378 kg/m^3). The sample thickness (L) was measured to be 40.1 ± 0.2 mm. For samples with the same amount of rice bran, those with higher adhesive content demonstrate higher density.

3.2 Sound Absorption Coefficient Spectra

The normal-incident SAC spectra measured by the two-microphone impedance tube method are given in the frequency range of 100 to 5,000 Hz. The SAC spectra describe how efficiently the samples can absorb sound at a specific frequency range. SAC values vary from zero to one, representing no absorption and total absorption, respectively. The SAC spectra of RB-a and RB-b with zero air gap are illustrated in Figures 5 and 6, respectively.

All rice bran samples exhibit the characteristics of a porous-type sound absorber where the SAC is considerably low at low frequency, and then suddenly rises until it reaches a point where the SAC becomes virtually saturated. Samples with lower bulk densities (RB-a1, RB-a2, RB-b1, RB-b2, and RB-b3) also show peak-valley characteristics in the saturation region of their SACs, as seen in previous literature [6,9,25]. The characteristics

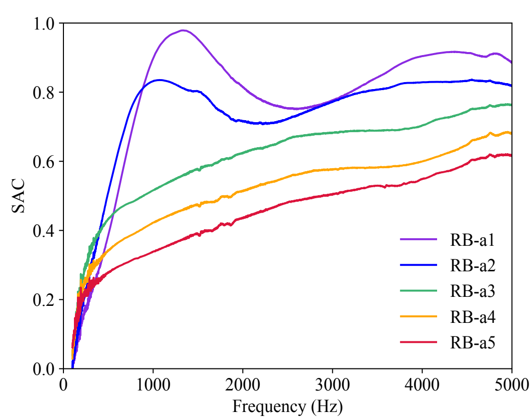

Figure 5. Normal-incident SAC spectra of RB-a samples at zero air gap (D_{UF} = 233 kg/m^3).

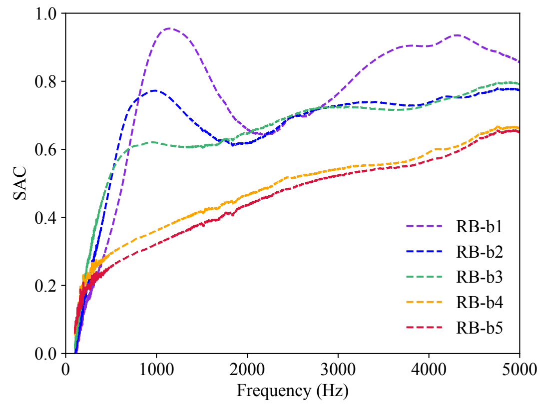

Figure 6. Normal-incident SAC spectra of RB-b samples at zero air gap (D_{UF} = 311 kg/m^3).

of these peaks and valleys depend on the loss of sound wave energy through viscous and thermal dissipation, as described in the semi-phenomenological Johnson-Champoux-Allard (JCA) model [14,27]. More details on this model can be found in subsection 3.3.

The noise reduction coefficient (NRC) of a sample is estimated by arithmetically averaging the SACs at 250, 500, 1000, and 2000 Hz [28]. Table 1 presents the NRC values. It demonstrates that samples with lower rice bran contents have NRCs greater than 0.47 ($D_{RB} \leq 253$). On the other hand, NRCs for samples with higher rice bran content ($D_{RB} > 253$) range between 0.30 and 0.40. The next subsection will describe the effects of non-acoustic parameters on the material's sound absorption ability.

3.3 Estimation of Non-acoustic Parameters

The Johnson-Champoux-Allard-Pride-Lafarge (JCAPL) model [14,27,29,30] is a semi-phenomenological model that has been proposed as a useful tool for predicting the sound absorption behavior of porous materials with a rigid frame and non-uniform pores. However, the practical application of this model has been limited due to the difficulties in accurately determining its original non-acoustic parameters. In this study, we have chosen to utilize the Johnson-Champoux-Allard (JCA) model [14,27] as an alternative. While the JCA model is not as comprehensive as the JCA-PL model, it has been widely used in the many literatures and has been shown to be effective in predicting the sound absorption behavior of some materials [31,32]. Five non-acoustic parameters are geometrical components of the JCA model include flow resistivity (σ), porosity (ϕ), tortuosity (α_∞), viscous characteristic length (Λ), and thermal characteristic length (Λ'). Equivalent dynamic density (ρ_{eq}) and equivalent dynamic bulk modulus (K_{eq}) of the airborne sound wave inside the porous absorber with rigid frame can be written as follows:

$$\rho_{\mathrm{eq}}(\omega) = \frac{\alpha_\infty \rho_0}{\phi}\left[1 + \frac{\sigma\phi}{j\omega\rho_0\alpha_\infty}\left(1 + \frac{4j\alpha_\infty^2\eta\omega\rho_0}{(\sigma\Lambda\phi)^2}\right)^{1/2}\right] \tag{6}$$

$$K_{\mathrm{eq}}(\omega) = \frac{\gamma P_0}{\phi}\left(\gamma - (\gamma - 1)\left[1 + \frac{\sigma\phi}{j\omega\rho_0\alpha_\infty N_{PR}}\left(1 + \frac{4j\alpha_\infty^2\eta N_{PR}\omega\rho_0}{(\sigma'\Lambda'\phi)^2}\right)^{1/2}\right]^{-1}\right)^{-1} \tag{7}$$

$$\sigma' = \frac{8\eta\alpha_\infty}{\Lambda'^2\phi} \tag{8}$$

where ω is the sound wave's angular frequency, ρ_0 is the density of the air, γ is the specific heat ratio of the air, η is the dynamic viscosity of the air, P_0 is the atmospheric pressure, and N_{PR} is Prandtl number. The complex wave number (k_c) and characteristic impedance (Z_c) can be calculated using:

$$k_{\mathrm{c}}(\omega) = \omega\sqrt{\frac{\rho_{\mathrm{eq}}(\omega)}{K_{\mathrm{eq}}(\omega)}} \tag{9}$$

$$Z_{\mathrm{c}}(\omega) = \sqrt{\rho_{\mathrm{eq}}(\omega)K_{\mathrm{eq}}(\omega)} \tag{10}$$

The transfer matrix method is a convenient tool for estimating the acoustic properties of multilayer absorbers [33]. In this study, we used this method to analyze the SAC spectra of a porous layer backed by an air gap (air layer). The transfer matrixes of the two layers including porous absorber (T_{porous}) and air gap (T_{airgap}) can be expressed as follows [34]:

$$T_{\mathrm{porous}} = \begin{bmatrix} \cos(k_{\mathrm{c}}d) & jZ_{\mathrm{c}}\sin(k_{\mathrm{c}}d) \\ j\sin(k_{\mathrm{c}}d)/Z_{\mathrm{c}} & \cos(k_{\mathrm{c}}d) \end{bmatrix} \tag{11}$$

$$T_{\mathrm{airgap}} = \begin{bmatrix} \cos(k_0 a) & jZ_0\sin(k_0 a) \\ j\sin(k_0 a)/Z_0 & \cos(k_0 a) \end{bmatrix} \tag{12}$$

$$T_{\mathrm{total}} = \prod_{i=1}^{2} T_{\mathrm{i}} = T_{\mathrm{porous}} \cdot T_{\mathrm{airgap}} = \begin{bmatrix} T_{11} & T_{12} \\ T_{21} & T_{22} \end{bmatrix} \tag{13}$$

where k_0 and Z_0 are the complex wave number and characteristic impedance of the air, d is sample thickness, and a is the distance of the air gap. Finally, the surface impedance (Z_S) of the combination of the porous absorber and airgap can be expressed as follows:

$$\mathrm{Z_s} = T_{11}/T_{21} \tag{14}$$

$$\mathrm{SAC} = 1 - \left|\frac{Z_{\mathrm{s}} - \rho_0 c_0}{Z_{\mathrm{s}} + \rho_0 c_0}\right|^2 \tag{15}$$

The expression provided in Eq.15 will be utilized as the mathematical model for least-squares fitting of SAC spectra of samples at concurrently zero, 20, and 40 mm air gaps. The fittings between mathematical and experimental results are illustrated in Figures 7 and 8. The optimized non-acoustic parameters are presented in Table 2.

In the theory of sound propagation in porous materials with elastic frames, described

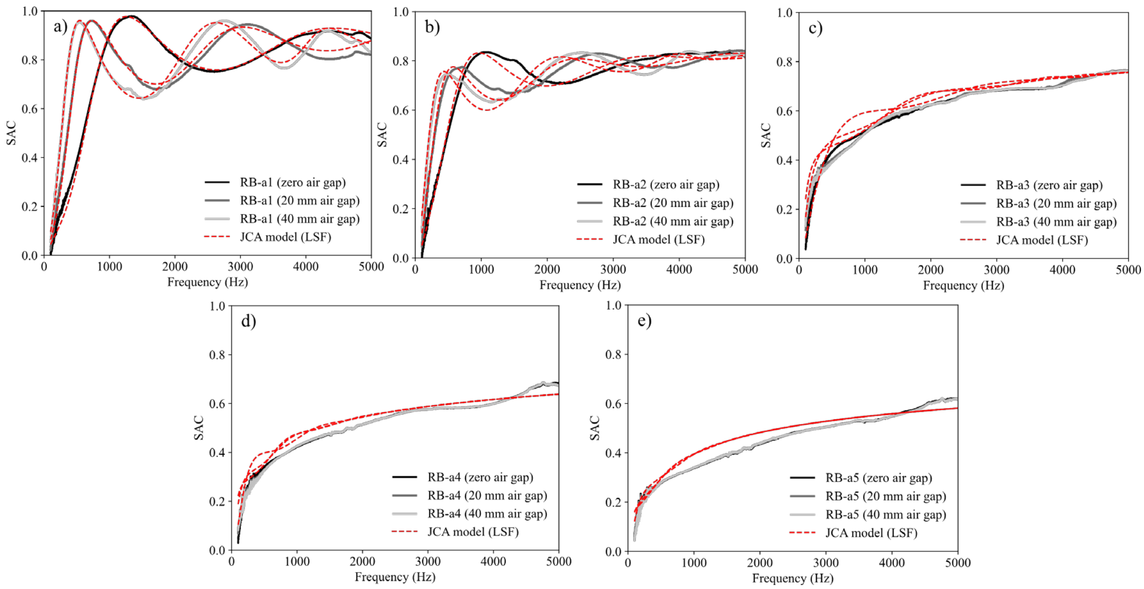

Figure 7. Experimental SAC spectra at various air gaps with calculation curves obtained from the JCA equivalent fluid model and transfer matrix method for RB-a1 a), RB-a2 b), RB-a3 c), RB-a4 d), and RB-a5 e).

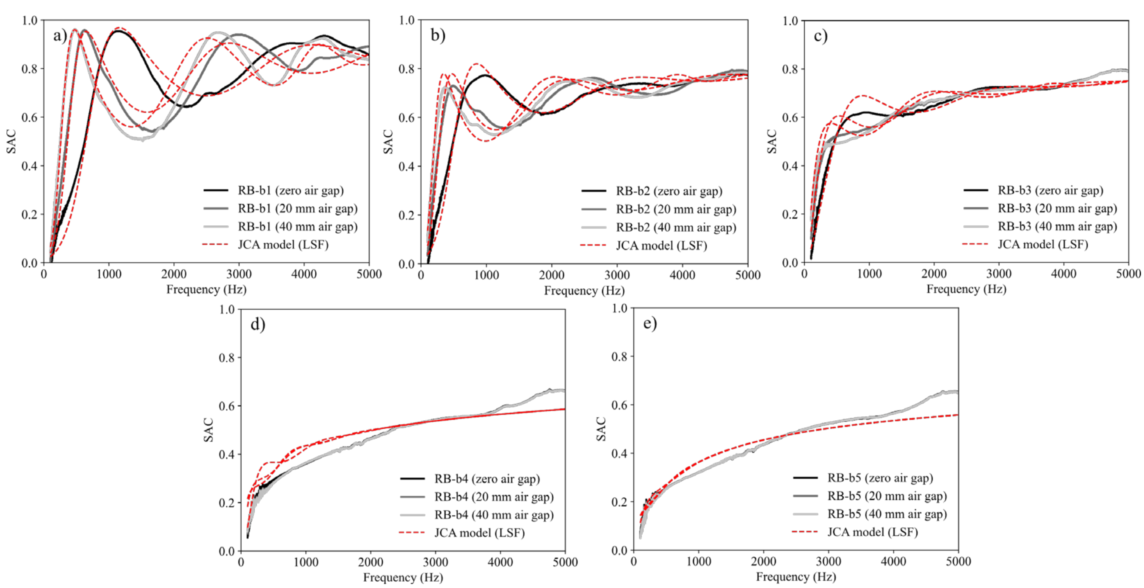

Figure 8. Experimental SAC spectra at various air gaps with calculation curves obtained from the JCA model and transfer matrix method for RB-b1 a), RB-b2 b), RB-b3 c), RB-b4 d), and RB-b5 e).

by Biot [35,36], there are two compressive waves that couple and propagate through the frame and pores. At lower frequencies, the air flow in the pores follows a Poisson-type pattern, with the fastest flow occurring at the center of the pore and decreasing towards the pore walls. At higher frequencies, the fluid in the center of the pores flows at the same velocity as an ideal fluid, while the fluid at the outer edges of the pores remains attached to the pore walls [36,37]. The layer of air at the outer edge of the pores is equal to the viscous skin depth (δ), as given in the equation below:

$$\delta = \left(\frac{2\eta}{2\pi f \rho_0}\right)^{1/2} \tag{16}$$

The transition occurs when the viscous skin depth is smaller than the diameter of smallest part of the connected pore network (pore interconnection). The transition between these two regimes is known as the Biot characteristic frequency or the decoupling frequency [30,36], given by:

$$f_c = \frac{\phi^2 \sigma}{2\pi \alpha_\infty \rho_0} \tag{17}$$

At frequencies above the f_c, one compressive wave becomes a frame-borne wave (mechanical wave) while the other becomes an airborne wave (acoustical wave). The decoupling between these two waves occurs above the f_c, at which point the frame can be treated as a rigid frame [33,35]. This can be explained using the semi-phenomenological JCA model. For the rigid frame model, the viscous skin depth at the Biot characteristic frequency (δ_c) should be approximately equal to the diameter of the pore interconnection, which is around twice the viscous characteristic length ($D \approx 2\Lambda$) [14]. This means that should be $\delta_c/2$ approximately equal to the viscous characteristic length ($\delta_c/2 \approx \Lambda$) for the rigid frame model. The calculated f_c and $\delta_c/2$ of all samples are displayed in Table 2.

From Table 2, the porosity (ϕ), viscous characteristic length (Λ), and thermal characteristic lengths (Λ') of both RB-a and RB-b are lower for the samples that include a higher proportion of RB. It has been observed that the thermal characteristic length directly correlates with the size of pores [27], while the viscous characteristic length shows a direct variation with pore interconnections [14]. Based on this information, it can be concluded that samples with higher RB contents tend to have smaller pores and interconnections, as evidenced by the lower values of fitted Λ and Λ' for these samples. The tortuosity (α_∞) is higher than 1 for low density samples including RB-a1 and RB-b1.

The SAC measurement was conducted within the frequency range around f_c for RB-a1, RB-a2, RB-b1, RB-b2, and RB-b3. In contrast, f_c for RB-a3, RB-a4, RB-a5, RB-b4, and RB-b5 exceeded the maximum measured frequency of 5,000 Hz. The calculated values of $\delta_c/2$ for most samples were similar to their fitted Λ values. For RB-a4, RB-a5, RB-b4, and RB-b5, the values of $\delta_c/2$ were approximately twice the size of the fitted Λ, but they are still in the same order of magnitude. Bardot et al. [38] have demonstrated that the rigid frame model (JCA) is acceptable for predicting the acoustical properties of some porous materials. It provides a good prediction not only at frequencies larger than the Biot characteristic frequency, but also at much lower frequencies that are generally explained using the full-phenomenological Biot model. Utilizing the Biot model to analyze the acoustic behavior of porous materials with high f_c in future studies is an intriguing avenue for exploration.

Flow resistivity is the only parameter that is clearly in direct variation with the RB content. According to the study of Bies-Hansen [39], materials with higher bulk density have higher flow resistivity. In the case of rice bran composites, although having a higher bulk density, RB-b with the same amount of rice bran demonstrates a lower flow resistivity than its RB-a counterpart. It suggests that bulk density alone is not the only component that should be considered when estimating the flow resistivity of composites; other parameters should also be considered. The empirical expression of the SAC will be explained based on the values of the material's flow resistivity in subsection 3.5.

The following subsection delves into the effect of uncertainty on the experimental results. Uncertainty of SAC was calculated using a multivariate method, as described by Schultz et al [40,41]. Figure 9 presents the experimental results along with their uncertainties and the SAC estimates derived from the JCA model.

3.4 Uncertainty Analysis

The uncertainty analysis in this study was based on the methodology described by Schultz *et al.* [40,41] where the transfer function (H_{12}) was measured using two microphones method, as defined by Eq. 4. To estimate the uncertainty of the reflection coefficient (R), a multivariate method [41] was employed, considering that the reflection coefficient consists of both real and imaginary components, which are considered bivariate. The multivariate method was used to propagate the uncertainty estimates using:

$$\boldsymbol{s}_{\mathrm{R}} = \boldsymbol{J}_{\mathrm{R}} \boldsymbol{s}_{\mathrm{H}} \boldsymbol{J}_{R}^{T} \tag{18}$$

where $\boldsymbol{s}_{\mathrm{R}}$, $\boldsymbol{s}_{\mathrm{H}}$ are the sample covariance matrix of reflection coefficient and transfer function, respectively. The covariance matrix, $\boldsymbol{s}_{\mathrm{H}}$ consist of variances and covariances of five factors including real part (H_{R}) and imaginary part (H_{I}) of the transfer function, distances (l, s), and temperature (T). $\boldsymbol{J}_R$ is the Jacobian matrix for the reflection coefficient while $\boldsymbol{J}_{\mathrm{R}}^{\mathrm{T}}$ is the transpose matrix of $\boldsymbol{J}_R$ as described in [40]. The uncertainty of reflection coefficient can be estimated from:

$$U_{\mathrm{R}} = k_{\mathrm{cf}} u_{\mathrm{R}} \tag{19}$$

where U_{R} represents the confidence level estimates of the uncertainty of reflection coefficient, and u_R is the standard deviation obtained from the square root of the diagonal elements of sample covariance matrix $\boldsymbol{s}_{\mathrm{R}}$. In the same way, k_{cf} is the

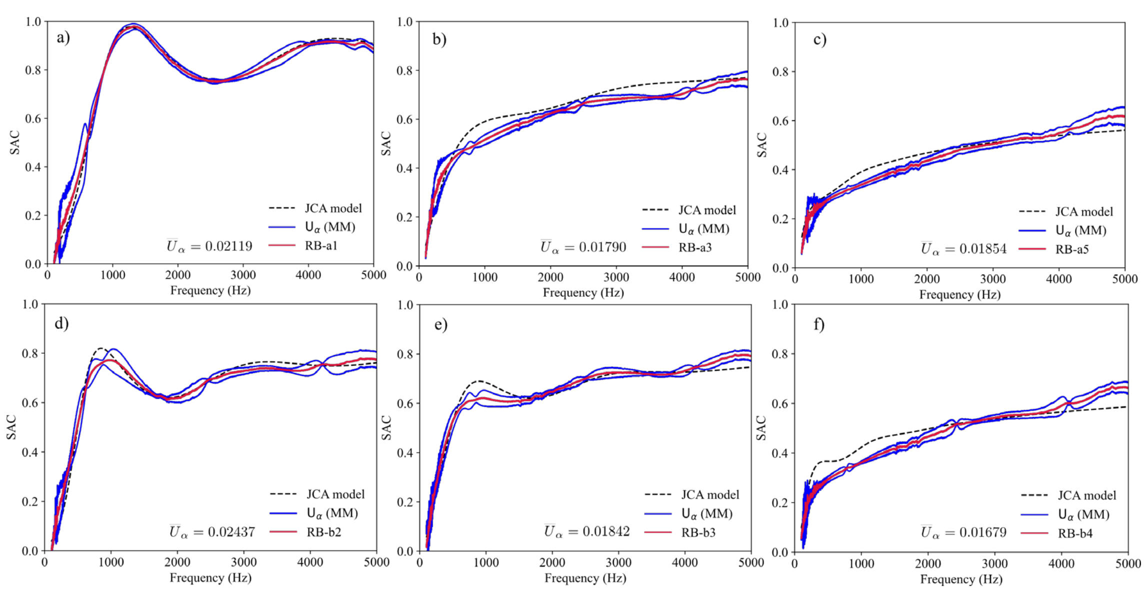

Figure 9. Experimental SAC spectra (red) with uncertainty (blue) and calculated SAC spectra from the JCA model (black-dashed) for RB-a1 a), RB-a3 b), RB-a5 c), RB-b2 d), RB-b3 e), and RB-b4 f).

coverage factor defined by:

$$k_{\mathrm{cf}} = \left(\frac{\nu_{\mathrm{eff}} p}{\nu_{\mathrm{eff}} + 1 - p} F_{p,\nu_{\mathrm{eff}}+1-p,\alpha}\right)^{1/2} \quad (20)$$

where $F_{p,\nu_{\mathrm{eff}}+1-p,\alpha}$ is the F distribution with p variate ($p = 2$, for real part and imaginary part of the transfer function), and $\nu_{\mathrm{eff}} + 1 - p$ degree of freedom for the probability $1 - \alpha$ [40,41]. ν_{eff} is the effective number of degrees of freedom which can be determined as mentioned by Willink and Hall [42]. The uncertainty of SAC (U_{α}) can be estimated from the method of partial derivatives as:

$$U_{\alpha} = \sqrt{\left(\frac{\partial \alpha}{\partial R_{\mathrm{R}}} \cdot U_{\mathrm{R_R}}\right)^2 + \left(\frac{\partial \alpha}{\partial R_{\mathrm{I}}} \cdot U_{\mathrm{R_I}}\right)^2} \quad (21)$$

where α is the SAC described in Eq. 5. $U_{\mathrm{R_R}}$ and $U_{\mathrm{R_I}}$ are the real part and imaginary part of U_{R}. The uncertainties of SAC with 95% confidence level of some samples are displayed in Figure 9. The SAC estimated from JCA model are shown in comparison with experimental SAC with U_{α}.

To reduce the level of uncertainty, it is crucial to maintain the consistency of the samples preparation process. However, this can be challenging with natural materials, as multiple uncontrollable factors such as grain size and shape can affect the consistency of the samples. An alternative approach is to optimize other related factors, such as ambient temperature (*T*), microphone spacing (*s*), and distance between the sample and nearest microphone (l). As suggested by Schultz *et al.* [40], the random uncertainty caused by temperature can be diminished by limiting the duration of the test. Similarly, the uncertainty due to distances l and *s* can be reduced by avoiding measurement at the frequency where $k_0 s = n\pi$.

The previous studies [40,43] mentioned that the uncertainty in the frequency peaks occurs when $k_0 s = n\pi$. In this study, the first peak ($n = 1$) was calculated to be approximately 6,000 Hz, which was higher than the maximum frequency used in the experiment. From Figure 9, the results of the JCA model for estimating SAC (black-dashed) were in good agreement with experimental results (red) with uncertainty (blue) in limited frequency ranges. In this study, materials with higher porosity tend to behave following the JCA model (such as RB-a1 and RB-b2), while materials with lower porosity may not show good agreement with the JCA model predictions in some frequency ranges (such as RB-b4). This suggests that there are additional factors affecting the acoustic behavior of materials with low porosity that are not included in the semi-phenomenological model such as the JCA model. Further research is needed to understand sound absorption behavior of low-porosity porous materials, as they may have potential as both sound absorbers and sound insulators [6].

The following subsection outlines the empirical model for determining the SAC using the material's flow resistivity. The newly developed empirical model was utilized to predict the SAC of rice bran composites and the results were compared to those obtained from the conventional Delany-Bazley model [16], as depicted in Figure 11.

3.5 An Empirical Model for the Sound Absorption Coefficient of Rice Bran Composites

Garai and Pompoli [17] demonstrated that the flow resistivity of the polyester fiber has a power-law relation with the material bulk density based on the Bies - Hansen model. However, it cannot be applicable for rice bran composites as RB-b with the same amount of rice bran demonstrates a lower flow resistivity than its RB-a counterpart. In the case of rice bran composites, we assume that the mass-per-volume ratios of the adhesive (D_{UF}) also have power-law relations with the flow resistivity. This is performed in place of considering the sample bulk density. To estimate the flow resistivity, Bies - Hansen model was modified to match the condition of composites containing two components. By optimizing the free parameters, *A*, *B*, and *C* using the least-square method on the flow resistivity from Table 2 and sample density from Table 1, the empirical model

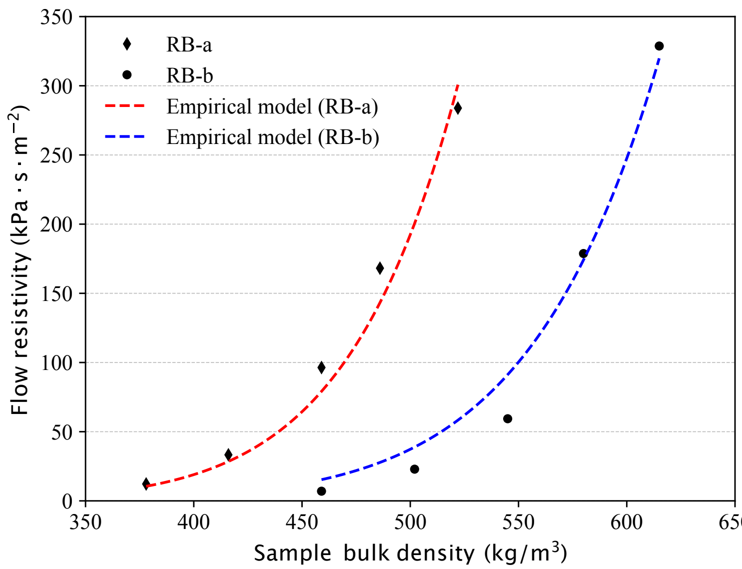

Figure 10. The experimental and calculated flow resistivity based on the empirical model described in Eq.22.

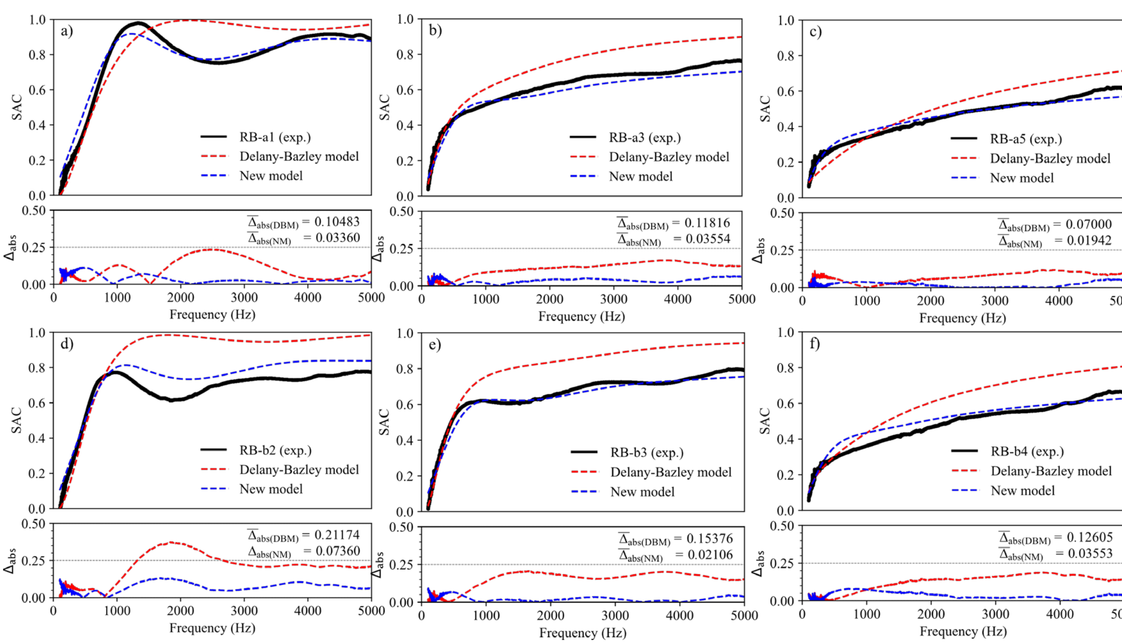

Figure 11. Comparison between experimental SACs and the values estimated from two empirical models (the Delany-Bazley model and the new model) for RB-a1 a), RB-a3 b), RB-a5 c), RB-b2 d), RB-b3 e), and RB-b4 f).

can be acquired as follows:

$$\sigma_{\text{est}} = A(\rho_{\text{bulk}})^B (D_{\text{UF}})^C \tag{22}$$

where σ_{est} is the estimated flow resistivity. A, B, and C are the optimized parameters obtained from the least-square fitting of flow resistivity of rice bran samples. In this study, A, B, and C are optimized to be 6.167×10^{-10} , 10.381, and −5.703, respectively. The fitting results are shown in Figure 10.

According to Eq. 2, 3, and 22, they demonstrated that the amount of adhesive (D_{UF}) influences the porosity and flow resistivity of the samples, which ultimately affect their SACs.

The flow resistivity values acquired from the measurement, as presented in Table 2, are utilized in the process of estimating the empirical model of SAC. The predictive model for the normal-incident SAC has been derived from the power-law relation as described in the Delany-Bazley model [16] [31]. The Delany-Bazley expressions are displayed in Eq. 23 and 24:

The SAC of the predictive model can be estimated by substituting Eq. 25 in Eq. 15. The least-square method is used to obtain the optimal values of parameters C_1 to C_8 in Eq. 23 - 24. SAC spectra of all ten distinctive samples (RB-a1 ~ RB-b5) were used in the reverse estimation of the new empirical model. The parameters of the new model are described in Table 3.

$$Z_{\text{c}} = \rho_0 c_0 \left[1 + C_1 \left(\frac{\rho_0 f}{\sigma}\right)^{-C_2} - jC_3 \left(\frac{\rho_0 f}{\sigma}\right)^{-C_4}\right] \tag{23}$$

$$K_{\text{c}} = \omega / c_0 \left[1 + C_5 \left(\frac{\rho_0 f}{\sigma}\right)^{-C_6} - jC_7 \left(\frac{\rho_0 f}{\sigma}\right)^{-C_8}\right] \tag{24}$$

$$Z_{\text{s}} = -jZ_{\text{c}} \cot(K_{\text{c}} d) \tag{25}$$

Figure 11 compares the estimates of SAC acquired from the new model to that obtained from the established Delany-Bazley model. The parameters, C_1 to C_8, of the Delany-Bazley model were obtained from the fitting of SAC spectra of numbers of glass wool absorbers with different thicknesses and densities [16]. The new model introduced in this study is obtained from the least-square fitting of the SAC of rice bran which has an entirely different geometry from the glass wool. As shown in Figure 11, the SAC calculated using the new model better matches the experimental results than the Delany-Bazley model. The Delany-Bazley model could predict the maximum values of SAC for some RB composites; however, it was incapable to predict the peak-valley characteristic of the SAC curve and overpredicted the SAC value at various frequency ranges [44]. In contrast, the prediction using the Delany-Bazley model provides improved fitting for samples with greater rice bran contents such as RB-a5 and RB-b4 as demonstrated in Figure 11. The average of absolute difference ($\overline{\Delta}_{\text{abs}}$) is derived from the arithmetic average of Δ_{abs} which is the difference between experimental and calculated SAC at a particular frequency. The smaller $\overline{\Delta}_{\text{abs}}$ signifies more model precision. In this study, $\overline{\Delta}_{\text{abs(DBM)}}$ is approximately 4.0 times greater

Table 3. The comparison between 8 parameters of the Delany-Bazley model and the new model.

Empirical Model	C_1	C_2	C_3	C_4	C_5	C_6	C_7	C_8
Delany-Bazley	0.057	0.754	0.087	0.732	0.098	0.700	0.189	0.595
New model	0.711	0.435	0.869	-0.803	-2.263	0.083	0.366	0.397

than $\overline{\Delta}_{\mathrm{abs(NM)}}$ for the majority of samples. It indicates that the new model is more capable of predicting the SAC values of rice bran samples than the Delany-Bazley model. The applications of the new model to other granular absorbers, as well as rice bran samples of varying thicknesses, have not yet been conducted. Since a range of granular materials is required for defining the unified empirical model for predicting the SAC of granular-type sound absorbers, it is intriguing for researchers to examine this topic in greater depth.

4. Conclusions

In this study, rice bran (RB) was used as the primary and structural component within a granular-type sound absorber with the urea-formaldehyde (UF) adhesive. Here are the most important findings from the two-microphone impedance tube measurement on samples with varied bulk densities from 378 to 615 kg/m^3, along with some interpretations:

• Rice bran composites as granular sound absorbers exhibit the fluctuated SAC spectra for samples with lower RB content where the highest NRC was observed to be 0.57. Meanwhile, the lowest NRC of 0.30 was found in the sample with relatively higher RB content.

• Fitting the experimental sound absorption coefficient (SAC) spectra to the semi-phenomenological Johnson-Champoux-Allard (JCA) equivalent fluid model using the least-squares approach yields some non-acoustic parameters. Porosity (ϕ), viscous characteristic length (Λ), and thermal characteristic length (Λ') tend to be lower in samples having higher RB contents. Flow resistivity (σ) is the sole parameter that rises as RB content increases.

• The new empirical model for SAC is based on the previous power-law relation presented by Delany and Bazley, in which the SAC is a function of flow resistivity alone. The new model (NM) predicts the SAC spectrum of RB composites with better precision than the prescribed Delany-Bazley model ($\overline{\Delta}_{\mathrm{abs(DBM)}} \approx 4.0\overline{\Delta}_{\mathrm{abs(NM)}}$).

• There is a need for further research to develop a comprehensive empirical model for predicting the sound absorption coefficient (SAC) of granular-type sound absorbers. This would involve the investigation of various granular materials and sample thicknesses. Another interesting avenue for exploration is the use of the Biot model, a fully phenomenological model, to analyze the acoustic behavior of materials with high Biot characteristic frequency (f_c). This topic presents a promising opportunity for future studies.

Acknowledgments

We are thankful to the Faculty of Science and Technology at Songkhla Rajabhat University, Thailand, for providing us with essential scientific tools and equipment.

Conflict of Interest Statement

The authors state that they have no known competing financial interests or personal ties that may have influenced the work presented in this study.

References

[1] Aso S. and Kinoshita R., *J. Text. Mach. Soc. Jpn.*, 1965; **18(11)**: 649–653. DOI 10.4188/transjtmsj1965b.18.t649.

[2] Kudo Y., Kotani M., Tomita M. and Aizawa Y., *J. Occup. Med. Toxicol.*, 2009; **4(5)**: 1–7. DOI 10.1186/1745-6673-4-5.

[3] Itewi M., *Am. J. Environ. Sci.*, 2011; **7(2)**: 161–165. DOI 10.3844/ajessp.2011.161.165.

[4] Koizumi T., Tsujiuchi N. and Adachi A., The Development of Sound Absorbing Materials using Natural Bamboo Fibers; in Brebbia C.A. and de Wilde W.P., eds., *High Performance Structures and Composites*, WIT Press, Southampton, 2002: 157–166.

[5] Hosseini M.H., Nor M.J.M., Ayub M. and Leman Z.A., *Appl. Acoust.*, 2010; **71(3)**: 241–249. DOI 10.1016/j.apacoust.2009.09.003.

[6] Chanlert P., Tongyoo S. and Rordrak C., *Appl. Acoust.*, 2022; **198**: 108984. DOI 10.1016/j.apacoust.2022.108984.

[7] Yang H.-S., Kim D.-J. and Kim H.-J., *Bioresour. Technol.*, 2003; **86(2)**: 117–121. DOI 10.1016/S0960-8524(02)00163-3.

[8] Kang C.-W., Oh S.-W., Lee T.-B., Kang W. and Matsumura J., *J. Wood Sci.*, 2012; **58(3)**: 273–278. DOI 10.1007/s10086-011-1243-5.

[9] Mamtaz H., Fouladi M.H., Nuawi M.Z., Namasivayam S.N., Ghassem M. and Al-Atabi M., *Appl. Acoust.*, 2017; **126**: 58–67. DOI 10.1016/j.apacoust.2017.05.012.

[10] Gross B.L. and Zhao Z., *Proc. Natl. Acad. Sci. U.S.A.*, 2014; **111(17)**: 6190–6197. DOI 10.1073/pnas.1308942110.

[11] Spaggiari M., Dall'Asta C., Galaverna G. and del Castillo Bilbao M. D., *Foods*, 2021; **10(1)**: 85. DOI 10.3390/foods10010085.

[12] Lee J., *Sci. Hortic-Amsterdam*, 2010; **124(3)**: 299–305. DOI 10.1016/j.scienta.2010.01.004.

[13] Andari R., *Scientiae Educatia*, 2018; **7(1)**: 11-20. DOI 10.24235/sc.educatia.v7i1.2517.

[14] Johnson D.L., Koplik J. and Dashen R., *J. Fluid Mech.*, 1987; **176**: 379–402. DOI 10.1017/S0022112087000727.

[15] Allard J.F. and Champoux Y., *J. Acoust. Soc. Am.*, 1992; **91(6)**: 3346–3353. DOI 10.1121/1.402824.

[16] Delany M.E. and Bazley E.N., *Appl. Acoust.*, 1970; **3(2)**: 105–116. DOI 10.1016/0003-682X(70)90031-9.

[17] Garai M. and Pompoli F., *Appl. Acoust.*, 2005; **66(12)**: 1383–1398. DOI 10.1016/j.apacoust.2005.04.008.

[18] Berardi U. and Iannace G., *Appl. Acoust.*, 2017; **115**: 131–138. DOI 10.1016/j.apacoust.2016.08.012.

[19] Norman G.R. and Newhouse M.T., *Can. Med. Assoc. J.*, 1986; **134**: 733–738.

[20] ISO-9053-1, Acoustics-Determination of airflow resistance-Part 1: Static airflow method, International Organization for Standardization, Geneva, 2018.

[21] Sreedhara S.S. and Tata N.R., *J. Eng. Fiber. Fabr.*, 2013; **8(4)**: 132–137. DOI 10.1177/155892501300800408.

[22] ASTM-E1050, Standard test method for impedance and absorption of acoustical materials using a tube, two microphones and a digital frequency analysis system, ASTM International, Pennsylvania, 1990.

[23] ISO-10534, Determination of sound absorption coefficient and impedance in impedance tubes : Part 2: Transfer-function method, International Organization for Standardization, Geneva, 1998.

[24] Koruk H., *Noise Control Eng. J.*, 2014; **62(4)**: 264–274. DOI 10.3397/1/376226.

[25] Chanlert P., Jintara A. and Manoma W., *Bioresources*, 2022; **17(4)**: 5612–5621. DOI 10.15376/biores.17.4.5612-5621.

[26] Wu Q., Ren M., Zhang X., Li C., Li T., Yang Z., et al., *LWT-Food Sci. Technol.*, 2021; **144**: 111230. DOI 10.1016/j.lwt.2021.111230.

[27] Champoux Y. and Allard J.F., *J. Appl. Phys.*, 1991; **70(4)**: 1975–1979. DOI 10.1063/1.349482.

[28] ISO-11654, Acoustics — sound absorbers for use in buildings — rating of sound absorption., International Organization for Standardization, Geneva, 1997.

[29] Lafarge D., Lemarinier P., Allard J.F. and Tarnow V., *J. Acoust. Soc. Am.*, 1997; **102(4)**: 1995–2006. DOI 10.1121/1.419690.

[30] Pride S.R., Morgan F.D. and Gangi A.F., *Phys. Rev. B*, 1993; **47(9)**: 4964–4978. DOI 10.1103/PhysRevB.47.4964.

[31] Soltani P., Taban E., Faridan M., Samaei S.E. and Amininasab S., *Appl. Acoust.*, 2020; **157**: 106999. DOI 10.1016/j.apacoust.2019.106999.

[32] Taban E., Amininasab S., Soltani P., Berardi U., Abdi D.D. and Samaei S.E., *J. Build. Eng.*, 2021; **41**: 102752. DOI 10.1016/j.jobe.2021.102752.

[33] Allard J.F. and Atalla N., *Propagation of Sound in Porous Media,* 1st Edn. Hoboken, New Jersey, USA: Wiley; 2009.

[34] Cai Z., Li X., Gai X., Zhang B. and Xing T., *Appl. Acoust.*, 2020; **170**: 107483. DOI 10.1016/j.apacoust.2020.107483.

[35] Biot M.A., *J. Acoust. Soc. Am.*, 1956; **28**: 168–178. DOI 10.1121/1.1908239.

[36] Biot M.A., *J. Acoust. Soc. Am.*, 1956; **28**: 179–191. DOI 10.1121/1.1908241.

[37] Sidler R., *J. Glaciol.*, 2015; **61(228)**: 789–798. DOI 10.3189/2015JoG15J040.

[38] Bardot A., Brouard B. and Allard J.F., *J. Appl. Phys.*, 1996; **79(11)**: 8223–8229. DOI 10.1063/1.362462.

[39] Bies D. A. and Hansen C.H., *Appl. Acoust.*, 1980; **13(5)**: 357–391. DOI 10.1016/0003-682X(80)90002-X.

[40] Schultz T., Sheplak M. and Cattafesta L.N., *J. Sound Vib.*, 2007; **304(1-2)**: 91–109. DOI 10.1016/j.jsv.2007.02.015.

[41] Schultz T., Sheplak M. and Cattafesta L.N., *J. Sound Vib.*, 2007; **305(1-2)**: 116–133. DOI 10.1016/j.jsv.2007.03.084.

[42] Willink R. and Hall B.D., *Metrologia*, 2002; **39**: 361–369. DOI 10.1088/0026-1394/39/4/5.

[43] Bodén H. and Åbom M., *J. Acoust. Soc. Am.*, 1986; **79(2)**: 541–549. DOI 10.1121/1.393542.

[44] Tuasikal J.A., Murata Y., Yoshida K., Harada T., Sato K., Daiguji H., et al., *AIAA J.*, 2022; **60(4)**: 2501–2521. DOI 10.2514/1.J060872.